Dendritic silver hierarchical structures for anode materials in Li ion batteries

Jing Li[1,2], Wenjun Fa[1,2], Hongxiao Zhao[1,2] ✉, Congxu Zhu[1,2], Huimin Jia[1,2], Longyan Gu[1,2]

[1]*Key Laboratory of Micro-Nano Materials for Energy Storage and Conversion of Henan Province, College of Advanced Materials and Energy, Institute of Surface Micro and Nano Materials, Xuchang University, Henan 461000, People's Republic of China*
[2]*Henan Joint International Research Laboratory of Nanomaterials for Energy and Catalysis, Xuchang University, Xuchang, Henan 461000, People's Republic of China*
✉ *E-mail: hxzhao0915@126.com*

Published in Micro & Nano Letters; Received on 22nd October 2018; Revised on 19th January 2019; Accepted on 26th March 2019

Dendritic silver hierarchical structures were prepared via a simple electrochemical deposition method in the presence of citric acid. The influence of the molar ratio of citric acid and $AgNO_3$, the deposition time and the deposition current on the crystalline and morphology of the products were studied by X-ray diffraction and scanning electron microscopy. Dendritic silver hierarchical structures consist of a long trunk with secondary branches, which grew in a parallel direction with a definite angle to the trunk. The average diameter of the trunk is 230–320 nm, that of the secondary branches is about 250 nm and the length of the branches is about 850 nm. The charge specific capacity of dendritic silver hierarchical structures was stable at around 250 mAh g^{-1} after 500 cycles at 0.1C. They also exhibited excellent rate capability at the various current rates from 0.1 to 5C.

1. Introduction: The conversion and storage of energy is very critical to the development of the society [1–6]. Among various electrical energy storage devices, Li ion batteries (LIBs) have drawn tremendous research for widely used in various electronic devices, such as video cameras, computers and mobile phones, due to their high energy density, good cycle life and high capacity [7, 8]. Being an important part of LIBs, the anode materials dominate the insertion–extraction process of Li ion and thus influence the electrochemical performance of the whole batteries [9]. So far, many anode materials, for instance, transition metal oxides or sulphides [10], metal or alloy [11] and graphene [12], have been intensively studied to satisfy the constantly increasing requirements for the electrode performance. Even so, it is still a key issue for exploring new materials as anode in LIBs.

In the past few decades, silver (Ag) has been frequently utilised in decorating of different electrode materials of LIBs to improve the electrochemical performance because of its high electrical conductivity, high specific capacity and low discharge–charge voltage [13–16]. In fact, Ag is a promising anode material since it is anti-corrosion and stable in various environments and can be easily obtained by a simple method [17–20]. However, the related work about the electrochemical performance of Ag is few. In [15], Ag–PEDOT core-shell nanocomposites were prepared and exhibited excellent electrochemical proprieties.

Many physical and chemical methods, including chemical reduction, hydrothermal method and electrochemical deposition, have been developed for the synthesis of silver nanomaterials [21–23]. Chemical reduction is a conventional method which mainly uses various reducing agents (such as $NaBH_4$) with or without surfactants. Polyol method, the reduction of $AgNO_3$ in ethylene glycol, is the most widely used chemical reduction and has been improved [24]. The high temperature and long reaction time were required in hydrothermal synthesis [25]. Compared with other techniques, the electrochemical deposition method is a very attractive pathway, due to its low cost, high productivity, easily controllable by potential or current, and available for large-scale production [26–28]. To the best of our knowledge, the electrochemical properties of silver as anode material in LIBs, which is synthesised via electrochemical deposition, have been not reported so far.

In this work, dendritic silver hierarchical structures were synthesised via a simple electrochemical deposition method. The molar ratio of citric acid and $AgNO_3$, the deposition time and the deposition current were investigated. The electrochemical properties of dendritic silver hierarchical structures as anode material of LIBs were explored.

2. Experimental: Silver nitrate ($AgNO_3$), citric acid ($C_6H_8O_7$), binder polyvinylidene fluoride (PVDF), N-methylpyrrolidone (NMP), ethylene carbonate ($C_3H_4O_3$), diethyl carbonate ($C_5H_{10}O_3$) and Lithium hexafluorophosphate ($LiPF_6$) were provided by Sinopharm Chemical Reagent Company (China). Conducive agent Timcal Graphite was provided by Imerys Graphite & Carbon. All the reagents are of analytical grade and were used without further purification. All solutions were prepared using double distilled water. Prior to all electrochemical synthesis experiments, the solution was degassed by bubbling N_2 for 20 min. The stainless steel substrate was cut and cleaned by sonication in ethanol for 20 min and dried by flowing air. Silver was electrodeposited on the previously treated substrate in a mixed solution of $AgNO_3$ and citric acid (pH = ~2.00) at room temperature. The electrodeposited was carried out by a constant current method under −1 to 1 V at the different current for the different time. The electrochemical deposition was carried out on an electrochemical system (CHI 660D) in a conventional three-electrode cell using stainless steel substrate as the working electrode, a Pt wire as the counter electrode and saturated calomel electrode as the reference electrode, respectively. The as-prepared Ag was washed several times using distilled water and dissolute ethanol and then dried in a vacuum at 60°C for 10 h.

The phases of the samples were characterised by X-ray diffraction (XRD, D8-Advance, Bruker Germany) with Cu Kα radiation ($\lambda = 1.54178$ Å, 40 KV, 40 mA) and a scan rate of 0.02°C s^{-1} between 10° to 90°. The morphologies of the products were examined by scanning electron microscope (SEM, ZEISS, LS15) at 15 kV. The nitrogen adsorption–desorption isotherms of the samples were measured at liquid nitrogen temperature using N_2 physical adsorption by the BET surface area analyser (Micromeritics Gemini 2380). The samples were scraped carefully from the substrate before measuring. Then these were dried at 80°C overnight before the analysis of the surface area.

All electrochemical tests were carried out at room temperature. The as-synthesised Ag was used as the anode active material and

the working electrode was prepared by mixing the products, conducive agent Timcal Graphite and PVDF at a weight ratio of 80:10:10 with NMP used as a solvent. The electrolyte solution was 1 mol L^{-1} $LiPF_6$ in ethylene carbonate/diethyl carbonate (EC/DEC, 1:1, v/v). The CR2016-type coin cell was assembled in the argon-filled glove box where H_2O and O_2 levels were both lower than 5 ppm and Li foil was used as the counter electrode. The charge–discharge curves were tested on muti-channel battery testing system (Land CT2001A, Wuhan Jinnuo Electronics Corp., China) at current densities of 0.1C (about 100 mA g^{-1}), 0.2, 0.5, 1, 2 and 5C in a potential range of 0.05–2.5 V.

3. Results and discussion: Figs. 1–3 show the typical XRD patterns of the products obtained at different ratios of raw materials, different deposition time and deposition current, respectively. All observed diffraction peaks of the products are in agreement with Ag (JCPDS Card No. 4-783, cubic, Fm3 m). The peaks at $2\theta = 38°$, 44°, 65°, 78° and 82° correlate to (111), (200), (220), (311) and (222) planes, respectively, of the Ag. No diffraction peaks of other phases or impurities were detected, confirming the high purity of as-synthesised Ag. The results indicated that the ratio of raw materials, deposition time and deposition current have no influence on the purity of the products. In addition, it is easily seen that the peak at 38° assigned to the (111) plane of Ag is very strong, which indicates that the as-synthesised materials were highly oriented perpendicularly to the [111] crystal axis [29]. Therefore, the prepared Ag is of high crystallinity, which can also be verified by the ultra-narrow (111) full width at half-maximum line width (<0.1°C) [30].

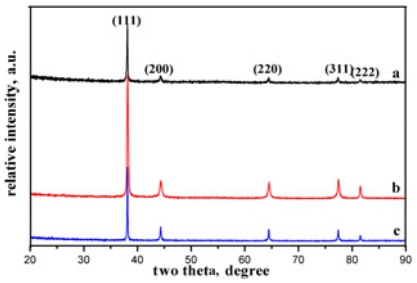

Fig. 1 *XRD pattern of Ag obtained at different ratio of raw materials*
a 2:1
b 1:1
c 1:2. Reaction time is 3000 s and current is 10 mA

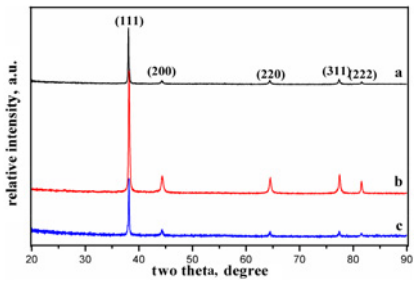

Fig. 2 *XRD pattern of Ag obtained at different reaction time*
a 1200 s
b 1500 s
c 3000 s. The ratio of raw materials is 2:1 and current is 10 mA

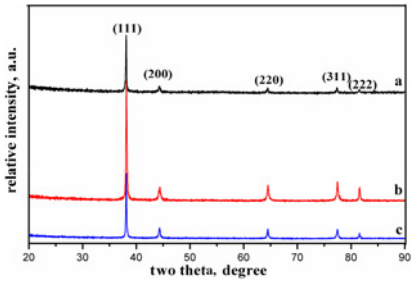

Fig. 3 *XRD pattern of Ag obtained at different current*
a 10 mA
b 5 mA
c 1 mA. The ratio of raw materials is 2:1 and Reaction time is 3000s

The morphologies of the products were characterised by SEM. Fig. 4 presents the morphologies of Ag at different molar ratios of raw materials. When the molar ratio of citric acid and silver nitrate is 1:2, only a few of the nanowires appear. When the molar ratio is 1:1, the nanowires become more and uniform, as shown in Fig. 4*b*. When the ratio is 2:1, the products become dendritic structures (Fig. 4*c*). So, the ratio (citric acid : silver nitrate) of 2:1 is selected. With the increase of citric acid, dendritic structures gradually formed because the added citric acid helped to stabilise the metal species and control the diffusion of silver ions by the formation of metal citrate complexes. The restricted diffusional mass transport of silver ions can limit the aggregates caused by the random diffusion of the particles and so the dendrites are obtained [31].

Deposition time also plays a key role on the morphology of the products. From Fig. 5*a*, it can be clearly seen that there are irregular nanorod structures in the first 1200 s. Some hierarchical structures are formed with a prolonged time of up to 1500 s. When the reaction time is prolonged to 3000 s (Fig. 5*c*), the morphologies of the samples are almost dendritic structures. So the dendritic

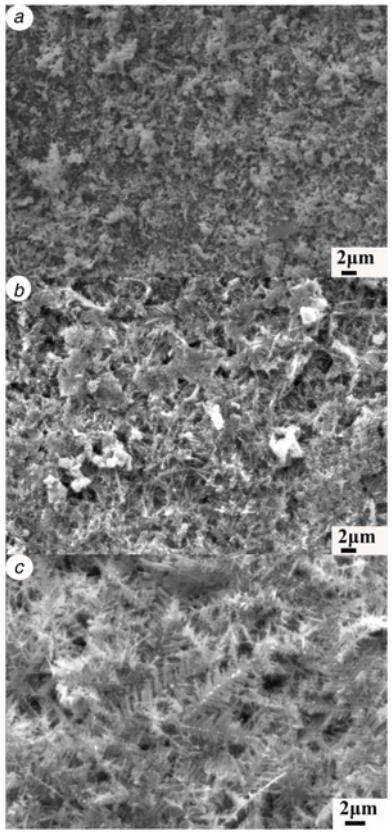

Fig. 4 *SEM images of Ag obtained at different molar ratio of citric acid/silver nitrate*
a 1:2
b 1:1
c 2:1

doi: 10.1049/mnl.2018.5648

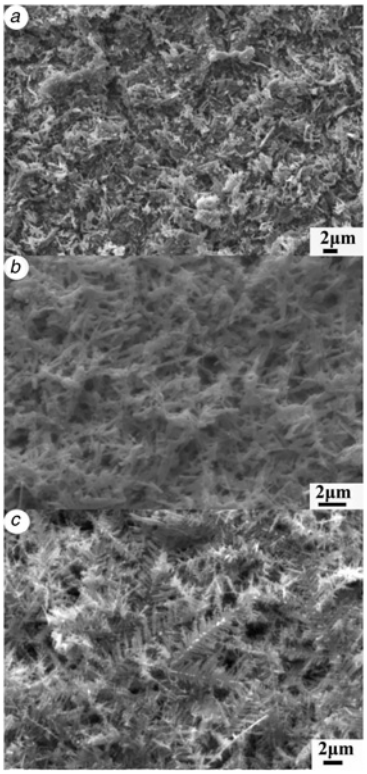

Fig. 5 *SEM images of Ag obtained at different reaction time*
a 1200 s
b 1500 s
c 3000 s

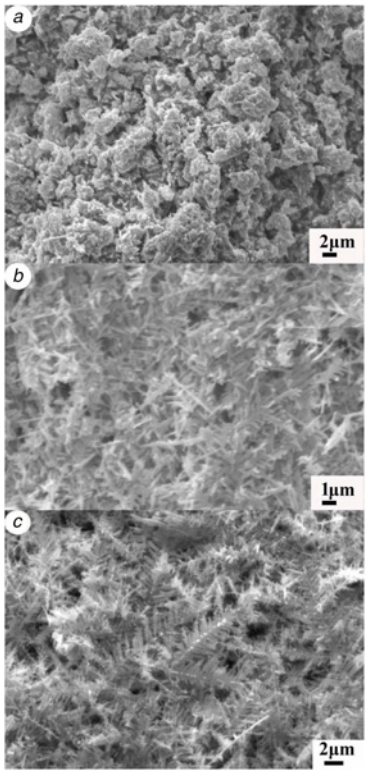

Fig. 6 *SEM images of Ag obtained at different current*
a 1 mA
b 5 mA
c 10 mA

structures depended upon the reaction time and 3000 s was chosen as the deposition time.

The influence of deposition current on the morphologies of the products was also studied and the SEM images were shown in Fig. 6. When the current was 1 mA, only particles with irregular sizes and agglomerations appear (Fig. 6*a*). When the current was elevated to 5 mA, there were some dendritic structures, as shown in Fig. 6*b*. As the current was further increased, the hierarchical Ag dendritic structures with high regularity were synthesised (Fig. 6*c*). So, we select 10 mA as the deposition current.

Based on the above results, the conditions of dendritic Ag hierarchical structures are the ratio of raw materials (citric acid : silver nitrate) 2:1, deposition time 3000 s and deposition current 10 mA. The dendritic structures were composed of some nanorods grown along the trunk in two opposite protrusion directions. The secondary branches were parallel with each other and emerged along certain angles to the central trunk. All the dendrites exhibited similar structures. The average diameter of the trunk were 230–320 nm and the secondary branches were about 250 nm. The length of the branches was about 850 nm. The formation of dendritic Ag hierarchical structures could be described by Diffusion-Limited Aggregation model as followed. In the early stage, the irregular-shaped particles formed and aggregated, as shown in SEM images. After the initial nucleation, these particles began to crystallise to form short rods and the initial growing direction was along (111) plane, which was the preferential growth direction [31, 32] and accordance with the results of XRD. Afterward, the rods were quickly grown up along the trunks. At the same time, some small particles or rods grown from particles were formed on the surface of the trunks. When the deposition time was prolonged, the growth speed of the trunk slowed down, while the small particles and rods grew quickly along their preferential growth directions under suitable reaction conditions, forming the secondary branches. At last, the growth speed of the branches slowed down and the dendritic hierarchical structures were formed [33]. The dendritic Ag hierarchical structures probably have a large specific surface area [34].

The representative charge–discharge curves for the 1st to 3rd of dendritic silver hierarchical structures recorded over the potential range between 0.05 and 2.5 V at a current density of 0.1°C (about 100 mA g^{-1}) are shown in Fig. 7*a*. The as-synthesised dendritic silver hierarchical structures showed long discharge voltage plateau at about 0.1 V, during which the dendritic silver hierarchical structures reacted with Li to form Li_xAg. The initial discharge and charge capacities are 809.1 and 515.5 mAh g^{-1}, which exceed the theoretical capacity of graphite, 372 mAh g^{-1}. The large irreversible capacity loss in the initial cycle is probably attributed to the formation of the solid electrolyte interface film and the irreversible decomposition of the electrolyte [31].

Fig. 7*b* shows the cycling performance of dendritic silver hierarchical structures in the voltage range of 2.5–0.05 V at 0.1C. Though the discharge capacities gradually decreased at first, the as-synthesised dendritic silver hierarchical structures demonstrated excellent reversible capacity. During the whole charge–discharge process, both the discharge and charge capacities of dendritic silver hierarchical structures were stable at about 250 mAh g^{-1}, which is considerably better than previously reported results [19]. Furthermore, from the third cycle onward, columbic efficiency is above 98%, indicating the excellent capacity retention of dendritic Ag hierarchical structures.

In addition to the charge–discharge capacity of dendritic silver hierarchical structures, the multiple-step galvanostatic charge–discharge was also investigated and the results were shown in Fig. 7*c*. The cells exhibit good rate performance with average discharge capacities of 850, 650 and 430 mAh g^{-1} at current densities of 0.1, 0.2, and 0.5C, respectively. Importantly, the discharge and charge capacities recover to 750 mAh g^{-1} when the current density returns to 0.1C. This demonstrated that even after

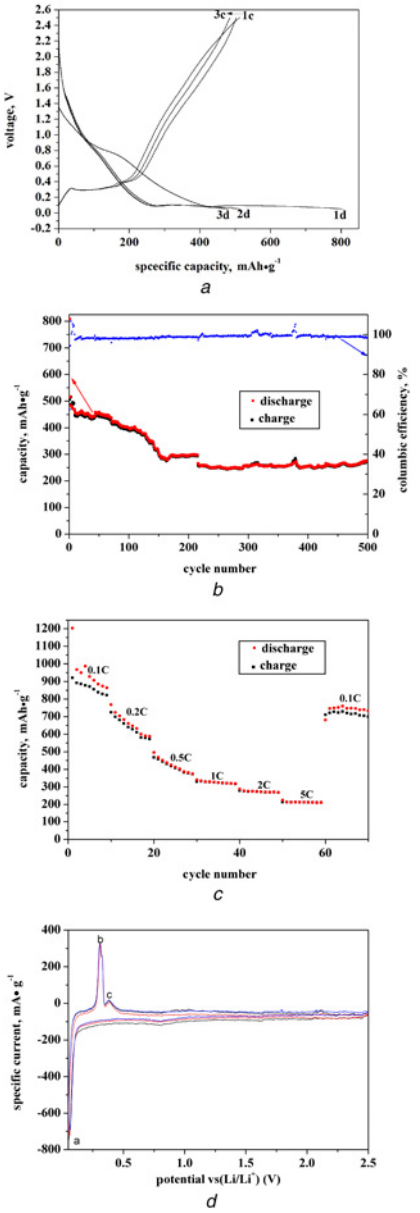

Fig. 7 *Electrochemical performance of dendriticsilver hierarchical structures*
a Charge–discharge curves of dendritic silver hierarchical structures recorded over the potential range between 0.05 and 2.5 V at 0.1C. The *n*th discharge and charge are denoted n_d and n_c, respectively
b Cyclic performance of dendritic silver hierarchical structures in the voltage range of 2.5–0.05 V at 100 mA g^{-1}
c Rate capability of dendritic silver hierarchical structures anode
d Cyclic voltammograms for Ag versus Li/Li^+ at scan rage of 0.05 mV/s

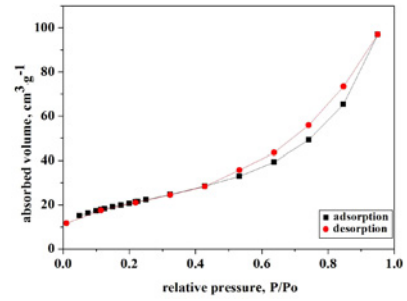

Fig. 8 *Nitrogen (N_2) adsorption–desorption isotherms of dendritic silver hierarchical structures*

discharge–charge cycles at 5000 mA g^{-1}, the electrode was not severely degraded and the cell still exhibited excellent cycling properties. Fig. 7*d* shows the 1st three CV curves of dendritic silver hierarchical structures at the scan rate of 0.05 mV s^{-1} in the potential range of 0.05–2.5 V versus Li/Li+. Silver starts to react at about 0.1 V, which is consistent with the pleat of charge–discharge curves. For the anodic scan at two peaks (about at 0.31 and 0.40 V) are observed, which points at a multi-step alloying mechanism. This cyclic voltammogram differs from and is similar with that reported by Wachtler *et al*. [35], who found a 3rd anodic peak at ca. 0.4 V. However, there are no redox peaks about the Ag alloying reaction, as shown in Fig. 7*d*. Therefore, the redox reactions should be negligible in this work. The cycles overlap well, indicating the superior reversibility of the electrochemical reaction.

The excellent electrochemical properties were attributed to the dendritic structures. The material of the branched structures has a high density of edges and corners, so that it has a larger specific surface area. The large specific surface area is beneficial to the electrochemical performances of the material. To explain the excellent electrochemical proprieties, the surface area of dendritic silver hierarchical structures was tested and the results were shown in Fig. 8. As we expected, the BET surface area of dendritic silver hierarchical structures is calculated to be 75.1711 m^2 g^{-1}, which favours the contacts between the electrolyte and active materials and more complete reactions during the charge–discharge process [35, 36].

4. Conclusion: In summary, dendritic silver hierarchical structures were successfully synthesised by a simple electrodeposition method. The influence of crucial reaction factors on the morphology and structure of the products, such as the ratio of raw materials, deposition current and time, has been investigated. The electrochemical performances of dendritic silver hierarchical structures as anode material for LIBs were evaluated by galvanostatic charge–discharge measurements. The stable anode materials with high performance were obtained and the columbic efficiency remained 98% up to 500 cycles. Dendritic Ag hierarchical structures also exhibited excellent rate capability at the various current rates from 0.1 to 5C. We anticipate that the dendritic silver hierarchical structures have potential application in rechargeable LIBs.

5. Acknowledgments: This work was supported by the National Natural Science Foundation of China (grant nos. 21673200 and U1604121), Henan Province Science and Technology Key Project (grant no. 162102410088), Program for Innovative Research Team in University of Henan Province (grant no. 19IRTSTHN026).

6 References

[1] He W.W., Kim H.K., Warner W.G., *ET AL.*: 'Photogenerated charge carriers and reactive oxygen species in ZnO/Au hybrid nanostructures with enhanced photocatalytic and antibacterial activity', *J. Am. Chem. Soc.*, 2014, **136**, pp. 750–757 (doi: 10.1021/ja410800y)
[2] Liu R., Zheng Z., Spurgeon J., *ET AL.*: 'Enhanced photoelectrochemical water-splitting performance of semiconductors by surface passivation layers', *Energy Environ. Sci.*, 2014, **7**, pp. 2504–2517 (doi: 10.1039/C4EE00450G)
[3] Wu G.D., Li P.J., Zhu C.X., *ET AL.*: 'Amorphous titanium oxide passivated lithium titanium phosphate electrode for high stable aqueous lithium ion batteries with oxygen tolerance', *Electrochim. Acta*, 2017, **246**, pp. 720–729 (doi: 10.1016/j.electacta.2017.06.093)
[4] Lei Y., Jia H.M., He W.W., *ET AL.*: 'Hybrid solar cells with outstanding short-circuit currents based on a room temperature soft-chemical strategy: the case of P3HT:Ag_2S', *J. Am. Chem. Soc.*, 2012, **134**, pp. 17392–17395 (doi: 10.1021/ja307521t)
[5] Wang J.J., Li L., Lei Y., *ET AL.*: 'Facile chemical solution transportation for direct recycling of iron oxide rust waste to hematite films', *ACS Sustain. Chem. Eng.*, 2018, **6**, pp. 12232–12240 (doi: 10.1021/acssuschemeng.8b02581)

[6] Jia H.M., He W.W., Chen X.W., *ET AL.*: 'In situ fabrication of chalcogenide nanoflake arrays for hybrid solar cells: the case of In_2S_3/poly (3-hexylthiophene)', *J. Mater. Chem.*, 2011, **21**, pp. 12824–12828 (doi: 10.1039/C1JM11539A)

[7] Huang G., Zhang L.L., Zhang F.F., *ET AL.*: 'Metal–organic framework derived Fe_2O_3@$NiCo_2O_4$ porous nanocages as anode materials for Li-ion batteries', *Nanoscale*, 2014, **6**, pp. 5509–5515 (doi: 10.1039/C3NR06041A)

[8] Yang S.L., Zhou X.F., Zhang J.G., *ET AL.*: 'Morphology-controlled solvothermal synthesis of $LiFePO_4$ as a cathode material for lithium-ion batteries', *J. Mater. Chem.*, 2010, **20**, pp. 8086–8091 (doi: 10.1039/C0JM01346C)

[9] Shen J.M., Feng Y.T.: 'Formation of flower-like carbon nanosheet aggregations and their electrochemical application', *J. Phys. Chem. C.*, 2008, **112**, pp. 13114–131120 (doi: 10.1021/jp802285c)

[10] Qiu D.F., Bu G., Zhao B., *ET AL.*: 'In situ growth of NiO nanoparticles on graphene as a high-performance anode material for lithium-ion battery anodes with enhanced strain accommodation', *RSC Adv.*, 2015, **5**, pp. 4385–4388 (doi: 10.1039/C4RA12416B)

[11] Hsu K.C., Liu C.E., Chen P.C., *ET AL.*: 'One-step vapor–solid reaction growth of Sn@C core–shell nanowires as an anode material for Li-ion batteries', *J. Mater. Chem.*, 2012, **22**, pp. 21533–21539 (doi: 10.1039/C2JM34654K)

[12] Zhang C., Jiao G.H., Kong F.J., *ET AL.*: 'Hierarchical Co_2P microspheres assembled from nanorods grown on reduced graphene oxide as anode material for lithium-ion batteries', *Appl. Surf. Sci.*, 2018, **459**, pp. 665–671 (doi: 10.1016/j.apsusc.2018.08.043)

[13] Fu L.J., Tang K., Chen C.C., *ET AL.*: 'Free-standing Ag/C coaxial hybrid electrodes as anodes for Li-ion batteries', *J. Maiera, Nanoscale*, 2013, **5**, pp. 11568–11571 (doi: 10.1039/c3nr03772j)

[14] Yun J.J., Wang Y., Gao T., *ET AL.*: 'In-situ electrochemical coating of Ag nanoparticles onto graphite electrode with enhanced performance for Li-ion batteries', *Electrochimi. Acta*, 2015, **155**, pp. 396–401 (doi: 10.1016/j.electacta.2014.12.129)

[15] Wu C.H., Hung F.Y., Lui T.S., *ET AL.*: 'Effects of Ag doping and annealing on the charge–discharge characteristics of $Al_{0.6}Si_{0.4}$ thin film anode', *Thin Solid Films*, 2013, **544**, pp. 28–32 (doi: 10.1016/j.tsf.2013.05.013)

[16] Gnanamuthu R.M., Prasanna K., Subburaj T., *ET AL.*: 'Silver effect of Co–Ni composite material on energy storage and structural behavior for Li-ion batteries', *Appl. Surf. Sci.*, 2013, **276**, pp. 433–436 (doi: 10.1016/j.apsusc.2013.03.111)

[17] Taillades G., Sarradin J.: 'Silver: high performance anode for thin film lithium ion batteries', *J. Power Sources.*, 2004, **125**, pp. 199–205 (doi: 10.1016/j.jpowsour.2003.07.004)

[18] Morales J., Sánchez L., Martín F., *ET AL.*: 'Synthesis, characterization, and electrochemical properties of nanocrystalline silver thin films obtained by spray pyrolysis', *J. Electrochem. Soc.*, 2004, **151**, pp. A151–A157 (doi: 10.1149/1.1632476)

[19] Jung H.R., Lee W.J.: 'Ag/poly(3,4-ethylenedioxythiophene) nanocomposites as anode materials for lithium ion battery', *Solid State Ion.*, 2011, **187**, pp. 50–57 (doi: 10.1016/j.ssi.2010.12.019)

[20] Wu X.D., Li H., Chen L.Q., *ET AL.*: 'Agglomeration and the surface passivating film of Ag nano-brush electrode in lithium batteries', *Solid State Ion.*, 2002, **149**, pp. 185–192 (doi: 10.1016/S0167-2738(02)00146-7)

[21] Haneda M., Towata A.: 'Catalytic performance of supported Ag nano-particles prepared by liquid phase chemical reduction for soot oxidation', *Catal. Today*, 2015, **242**, pp. 351–356 (doi: 10.1016/j.cattod.2014.05.044)

[22] Meléndrez M.F., Medina C., Solis-Pomar F., *ET AL.*: 'Quality and high yield synthesis of Ag nanowires by microwave-assisted hydrothermal method', *Nanoscale Res. Let.*, 2015, **10**, p. 48 (doi: 10.1186/s11671-015-0774-x)

[23] Xie W., Zheng Y.Y., Kuang J.C., *ET AL.*: 'Preparation of disperse silver particles by chemical reduction', *Russ. J. Phys. Chem. A*, 2016, **90**, pp. 848–855 (doi: 10.1134/S0036024416040324)

[24] Lim G.H., Lee S.J., Han I., *ET AL.*: 'Polyol synthesis of silver nanostructures: inducing the growth of nanowires by a heat-up process', *Chem. Phys. Lett.*., 2014, **602**, pp. 10–15 (doi: 10.1016/j.cplett.2014.04.012)

[25] Bao Z.H., Sun Z.H., Xiao M., *ET AL.*: 'Hydrothermal transformation from Au core–sulfide shell to Au nanoparticle-decorated sulfide hybrid nanostructures', *Nanoscale*, 2010, **2**, pp. 1650–1652 (doi: 10.1039/C0NR00302F)

[26] Li X.D., Li M.C., Cui P., *ET AL.*: 'Electrodeposition of Ag nanosheet-assembled microsphere@Ag dendrite core–shell hierarchical architectures and their application in SERS', *CrystEngComm.*, 2014, **16**, pp. 3834–3838 (doi: 10.1039/C3CE41946K)

[27] Chu J., Zhao Y., Li S.H., *ET AL.*: 'A highly-ordered and uniform sunflower-like dendritic silver nanocomplex array as reproducible SERS substrate', *RSC Adv.*, 2015, **5**, pp. 3860–3867 (doi: 10.1039/C4RA11151F)

[28] Al-Salman R., Endres F.: 'Template-assisted electrodeposition of SixGe1 – xnanowires with varying length and composition from two different ionic liquids', *J. Mater. Chem.*, 2009, **19**, pp. 7228–7231 (doi: 10.1039/B909265J)

[29] Su Z., Wang L., Grigorescu S., *ET AL.*: 'Hydrothermal growth of highly oriented single crystalline Ta_2O_5 nanorod arrays and their conversion to Ta3N5 for efficient solar driven water splitting', *Chem. Commun.*, 2014, **50**, pp. 15561–15564 (doi: 10.1039/C4CC05673F)

[30] Wu X., Bai H., Li C., *ET AL.*: 'Controlled one-step fabrication of highly oriented ZnO nanoneedle/nanorods arrays at near room temperature', *Chem. Commun.*, 2006, pp. 1655–1657 (doi: 10.1039/B516497D)

[31] Sivasubramanian R., Sangaranarayanan M.V.: 'Electrodeposition of silver nanostructures: from polygons to dendrites', *CrystEngComm.*, 2013, **15**, pp. 2052–2056 (doi: 10.1039/C3CE26886A)

[32] Alam M.M., Ji W., Luitel H.N., *ET AL.*: 'Template free synthesis of dendritic silver nanostructures and their application in surface-enhanced Raman scattering', *RSC Adv.*, 2014, **4**, pp. 52686–52689 (doi: 10.1039/C4RA10113H)

[33] Yang Q., Shen R.W., Zeng C.F., *ET AL.*: 'Controllable hydrothermal synthesis of 2D and 3D dendritic aluminum phosphate crystals', *CrystEngComm.*, 2013, **15**, pp. 4295–4302 (doi: 10.1039/C3CE40127H)

[34] Tanmay G., Pabitra D., Tapas K.C., *ET AL.*: 'Tilt boundary induced heteroepitaxy in chemically grown dendritic silver nanostructures on germanium and their optical properties', *Phys. Chem. Chem. Phys.*, 2014, **16**, pp. 16730–16739 (doi: 10.1039/C4CP01711K)

[35] Wachtler M., Winter M., Besenhard J.O., *ET AL.*: 'Anodic materials for rechargeable Li-batteries', *J. Power Sources*, 2002, **105**, pp. 151–160 (doi: 10.1016/S0378-7753(01)00934-X)

[36] Zhang Y., Jiang C., Zhuang S., *ET AL.*: 'Mesoporous In_2O_3 nanofibers assembled by ultrafine nanoparticles as a high capacity anode for Li-ion batteries', *RSC Adv.*, 2016, **6**, pp. 49782–49786 (doi: 10.1039/C6RA07804D)